# Active site imprinting on Ti oxocluster metal–organic frameworks for photocatalytic hydrogen release from formic acid

Alberto García-Baldoví, Raquel del Angel, Georges Mouchaham, Shanping Liu, Dong Fan, Guillaume Maurin, Sergio Navalón, Christian Serre, Hermenegildo Garcia

# Active site imprinting on Ti oxocluster metal-organic framework for the photocatalytic hydrogen release from formic acid

Alberto García-Baldoví,[a] Raquel Del Angel,[b] Georges Mouchaham,[b*] Shanping Liu,[c] Dong Fan,[c] Guillaume Maurin,[c] Sergio Navalón,[d] Christian Serre, [b*] Hermenegildo Garcia,[a*]

[a] Instituto Universitario de Tecnología Química, Consejo Superior de Investigaciones Científicas-Universitat Politècnica de València, Universitat Politècnica de Valencia, Av. De los Naranjos s/n, 46023 Valencia, Spain

[b] Institut des Matériaux Poreux de Paris, Ecole Normale Supérieure, ESPCI Paris, CNRS, PSL University, Paris, France

[c] ICGM, Univ. Montpellier, CNRS, ENSCM, Montpellier, France

[d] Chemistry Department, Universitat Politècnica de València, Av. De los Naranjos s/n, 46023 Valencia, Spain

**Abstract**

On-board hydrogen release from liquid organic carriers is a process that can make feasible the use of $H_2$ as transportation fuel. Formic acid is considered as one of the most convenient liquid hydrogen organic carriers, since it can be easily obtained from $CO_2$, it is water soluble and it makes unnecessary to recover the $H_2$-depleted byproducts. Compared to the more conventional thermal catalytic decomposition of formic acid, the use of light in

combination with a photocatalyst has been much less explored. Herein, we report a new paradigm in MOF photocatalysis with the use of a microporous titanium oxocluster based metal-organic framework (Ti-MOF) endowed by formate-imprinted active sites, namely MIP-177_LT (MIP stands for Materials from Institute of Porous Materials of Paris, LT for Low Temperature), as a highly efficient photocatalyst for $H_2$ release from formic acid without the need to neutralize acidity or the use sacrificial agents or noble metals. Noteworthy, a quantum efficiency of 22 % has been determined for the photocatalytic $H_2$ release that is highly remarkable for a non-toxic noble metal-free photocatalyst.

**Keywords**: Photocatalysis; liquid hydrogen organic carriers; on-board $H_2$ release from formic acid; imprinted MOFs as photocatalyst.

## Introduction

In the forthcoming decarbonized energy, hydrogen will play a key role as energy vector.[1] However, implementation of the hydrogen technology is hampered by several bottlenecks related to hydrogen generation from water using renewable energy, safe and adequate hydrogen storage and non-polluting hydrogen consumption. In the context of the use of hydrogen in transportation, one of the major problems is the low volumetric energy density of compressed hydrogen.[2] One approach to overcome this issue is the use of liquid organic compounds (known as *liquid organic hydrogen carriers*, LOHCs) that can release on-board hydrogen on demand.[3, 4] Among the requirements for an ideal LOHCs, the most important ones are easy synthesis, facile hydrogen release, lack of toxicity, water solubility and high percentage of hydrogen release. Thus, formic acid (HCOOH, FA) is among the most investigated LOHC not only owing to its hydrogen content (4.4 wt.%),[5] stability and non-toxic character, but also because its availability from biomass as well as from $CO_2$ hydrogenation. Besides, the HCOOH/$CO_2$ system can be considered as an ideal environmental-friendly system for hydrogen storage provided that $CO_2$ is obtained from air, in which case the whole hydrogen storage/hydrogen release cycle is $CO_2$ neutral. Indeed, dehydrogenation and re-hydrogenation reactions ($HCOOH \leftrightarrow H_2 + CO_2$; $\Delta G = -48.4$ kJ $mol^{-1}$) [6] can be considered as a neutral $CO_2$-footprint cycle.[5]

Catalytic FA decomposition at room temperature has been reported using noble metals,[6-10] making the process of low applicability. Other transition metals can also promote hydrogen release from FA,[11-15] but they require some heating, occur at slower rate and are much less efficient. In addition, due to the known dissolution of metals in acid

medium and the ability of FA to form soluble metal-coordination complexes, corrosion of the catalyst and/or metal leaching are some of the limitations generally encountered in such a process.[16] To circumvent this issue, hydrogen release measurements have been reported for formate salts,[17] but this makes again the process less attractive since no FA is directly used, but a derivative containing unwanted alkali metal ions or other charge compensating cations, such as $NH_4^+$. This makes necessary FA neutralization with bases.[18] Moreover, other common problem of FA decomposition is the occurrence in some degree of FA dehydration ($HCOOH \leftrightarrow H_2O + CO$; $\Delta G = -28.5$ kJ $mol^{-1}$) taking place in some extent concomitantly with FA dehydrogenation.[19] It appears that the monodentate binding mode of FA on the catalyst surface at the expense of bridging mode adsorption is more favorable for the unwanted dehydration reaction.[6] The presence of CO from FA dehydration, even in minute proportions, is highly detrimental for the use of the released $H_2$ in fuel cells, due to catalyst poisoning.[20] Therefore, a proper design of the active site to reach highly selective dehydrogenation reaction is desirable.

One alternative to conventional thermal catalysis that has been considerably less explored is the photocatalytic FA decomposition. Photocatalysis can promote FA decarboxylation.[21] In a general reaction mechanism, photogenerated holes abstract one electron from formic acid or formate giving HCOO· radical that decomposes spontaneously, giving a $CO_2$ molecule and a hydrogen atom.[21] Photogenerated electrons are consumed by $H^+$ forming another hydrogen atom. Typical photocatalysts for FA decomposition are $TiO_2$ materials in various crystalline phases, structural morphologies and dopants.[22-25] However, even when using $TiO_2$ as photocatalyst, noble metal co-catalysts such as Pt [26, 27], Au [23, 25]

and Pd [28] are generally employed to increase charge separation and to favor the occurrence of chemical reactions. Although much less studied, other photocatalysts besides $TiO_2$, either independently or as heterojunctions, have also been tested for the photocatalytic FA decomposition.[21] The list includes toxic CdS [29] or metal phosphides prepared using poisonous and hazardous phosphine,[30] as well as $BiVO_4$,[31] reduced graphene oxide[32-34] and carbon nitride.[35] Also in these cases, these photocatalysts contain in most cases noble metals to enhance their catalytic activity.

Metal-organic frameworks (MOFs) are becoming very attractive candidates for catalysis in general and, for photocatalysis in particular.[36-38] Thanks to the versatility of their hybrid (organic/inorganic) porous and highly ordered (crystalline) structure, their features can be finely tuned to deliver great catalytic performance with a minimal energetic penalty. MOFs have also been employed as passive hosts of active CdS, plasmonic Au@Pd or $In_2S_3$/Co(salen) photocatalysts for FA decomposition,[39-41] observing in some cases the evolution of a significant CO proportion,[39, 41] whose presence is highly detrimental for the operation of hydrogen fuel cells. In these examples MOFs are acting as porous supports with a negligible intrinsic activity. However, as far as we know MOFs by themselves have not been yet considered as candidates for hydrogen release from FA in the absence of any sacrificial agent.

MOF synthesis is a very active area of research.[42, 43] As an example of the various synthetic approaches offered by MOFs, there is a current trend in MOF synthesis of using, besides the organic building units (multitopic ligands) required to connect the inorganic building units (IBU), other organic additives known as modulators.[42] These modulators are

competing during the MOF synthesis with the structural ligands in terms of coordination with the metal ions of the IBU, allowing a better control of the nucleation process and, hence, on the overall crystallinity of the resulting MOF sample. Beyond their impact over the crystallization process, these modulators can induce the formation of structural defects that could be beneficial to enhance the MOF activity in various applications, particularly in catalysis and photocatalysis, by promoting accessible active metal sites and charge carrier trapping sites, respectively.[44, 45]

Among the various modulators reported, monotopic carboxylic acids and particularly FA are some of the preferred agents.[46, 47] Depending on the MOF structure, the nature of the building units, and the synthetic conditions, the modulator can either (i) replace the structural linker, leading a ligand defective structure, and/or (ii) occupy a free position inherently not affecting the structuring ligands. In both cases, the modulators can play a role to create potential accessible active sites. It occurred to us that FA as modulator can also be positively used to "*imprint*" in the resulting MOF structure an active site for the photocatalytic FA decomposition in the photoresponsive MOFs.

In this regard, Ti-MOFs are a particularly attractive sub-class of materials of most relevance as photocatalyst candidates, owing to their IBU constituted of Ti metal ions known for their photophysical response and redox photoactivity.[48] While in general transition metals with incompletely filled d orbitals undergo a fast d←d electronic relaxation of the excited states, $d^0$ or $d^{10}$ transition metals, like $Ti^{4+}$ or $Zn^{2+}$, not suffering from this deactivation pathway are photocatalytically more efficient.[48] Our hypothesis is that one of these Ti-MOFs, denoted MIP-177-LT,[49] prepared in FA as pure solvent under

solvothermal conditions should be particularly efficient for FA decomposition, due to the FA modulator templating during its synthesis.[49] MIP-177-LT with a robust 3D microporous structure of formula $Ti_{12}O_{15}(mdip)_3(formate)_6$ (mdip: methylene di-isophthalate), is built up of $Ti_{12}O_{15}$ oxoclusters as IBU, where the $Ti^{IV}$ ions are connected by $\mu_3$-oxo bridges, carboxylate groups of different mdip ligands and formate groups as depicted in Fig. 1.[49] As shown in this Figure, there are two types of formate groups. Half of them (highlighted in green) are linking two adjacent equatorial Ti ions in each $Ti_{12}$-oxocluster, and they are accessible through channels running along the *c*-axis. A second half (highlighted in yellow) are bridging two adjacent $Ti_{12}O_{15}$ clusters and they are not exposed to the micropores. MIP-177-LT exhibits also remarkable chemical stability, among the best MOFs, including stability against strong acids such concentrated HCl, sulfuric and nitric acids, *aqua regia* and even 6 M $H_3PO_4$ which has been of interest for proton conductivity [50] or release of nitric oxide in simulated body fluid conditions.[51]

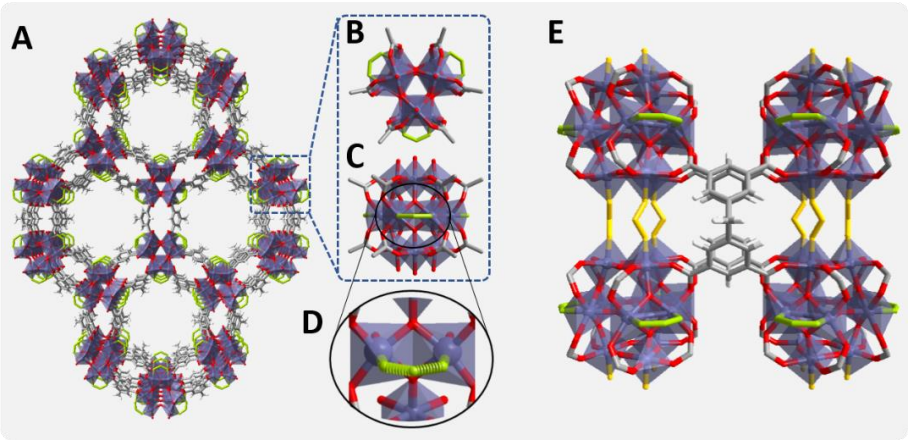


**Fig. 1. A**, Crystal structure of MIP-177-LT. **B** and **C**, $Ti_{12}O_{15}$ cluster showing non-bridging formates (equatorial) in green, top and side view, respectively. **D**, View of the equatorial formate-imprinted sites. **E**, View showing in yellow the bridging formates between two adjacent $Ti_{12}$ oxoclusters aligned along the *c*-axis..

Considering the remarkable photocatalytic activity of Ti-MOFs, the high chemical stability of MIP-177-LT to strong acids being prepared in FA at reflux temperature, it motivated us to consider this MOF as formate-*imprinted* catalyst to promote the photocatalytic hydrogen release from FA. Formate imprinting should make possible the recognition of FA by the active sites, fitting adequately in the structure. As it will be shown below, containing exclusively Ti as the only metal in the absence of noble metals, MIL-177-LT is a very efficient and stable photocatalyst for hydrogen release from aqueous solutions of FA, comparing favorably with other Ti- and Zr-containing MOFs and with conventional $TiO_2$ photocatalysts.

**Results and discussion.**

The concept of the present study is summarized in Fig. 2 in which key aspects, like formate molecular imprinting, structural stability against strongly corrosive acids, the presence of Ti oxoclusters and other features of MIP-177-LT have been highlighted. The synthesis of MIP-177-LT was performed as reported [49] from $Ti(^iPrO)_4$ as the molecular source of $Ti^{IV}$ and di(isophthalyl)methane ($H_4$mdip) as linker in FA as solvent under reflux conditions during 48 hours. MIP-177-LT synthesis is reliable and it can be scaled up to 100 g. The samples used for the present study exhibit the expected PXRD pattern, chemical composition and spectroscopic properties as reported before.[49] Fig. 3 shows XRD characterization data of the MIP-177-LT sample under study. Besides the MIP-177-LT, another MIL-177-LT sample was submitted to acid treatment (MIP-177-LT-AT), to remove formate groups coordinated on the Ti sites, while only slightly decreasing somehow the BET area of the material that

goes from 640 $m^2g^{-1}$ for MIP-177-LT to 560 $m^2g^{-1}$ for MIP-177-LT-AT. These two MOFs showed some differences in their optical properties, where a blue shift can be observed on the absorption onset wavelength in the diffuse reflectance UV-Vis absorption spectrum of MIP-177-LT-TA compared to MIP-177-LT (Fig. S1), probably due to the removal of oligomeric $TiO_x$ impurities occupying some pore space that could be present in MIP-177-LT. Additional characterization, including diffuse-reflectance optical spectra, diffraction patterns, $N_2$ and $CO_2$ adsorption/desorption isotherms and SEM images of the MIP-177-LT and MMIP-177-LT-TA samples used in the present study, including particle morphology and XPS data are presented also in Fig. S1. For the sake of comparison, this study was also completed with MIL-125(Ti) and UiO-66(Zr) taken as reference MOF photocatalysts and commercial P25 $TiO_2$.

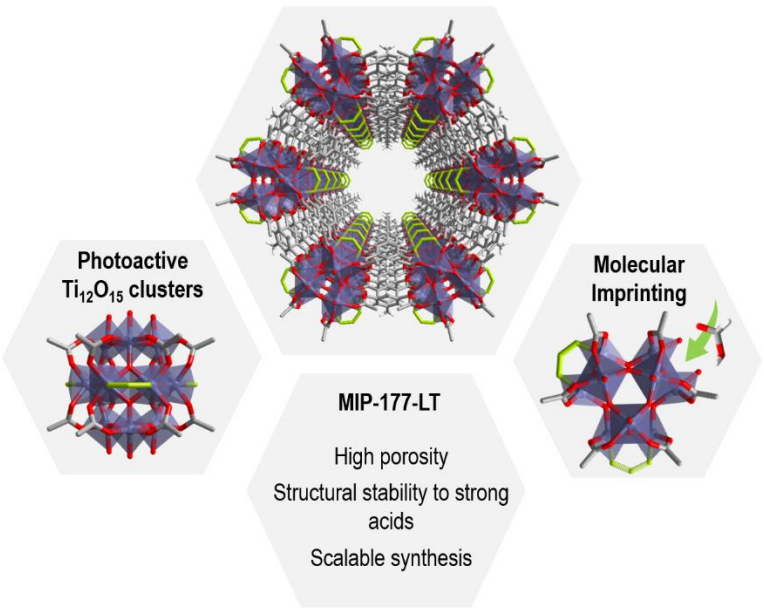


Fig. 2. MIP-177 optimum features for an effective photocatalytic $H_2$ release from FA.

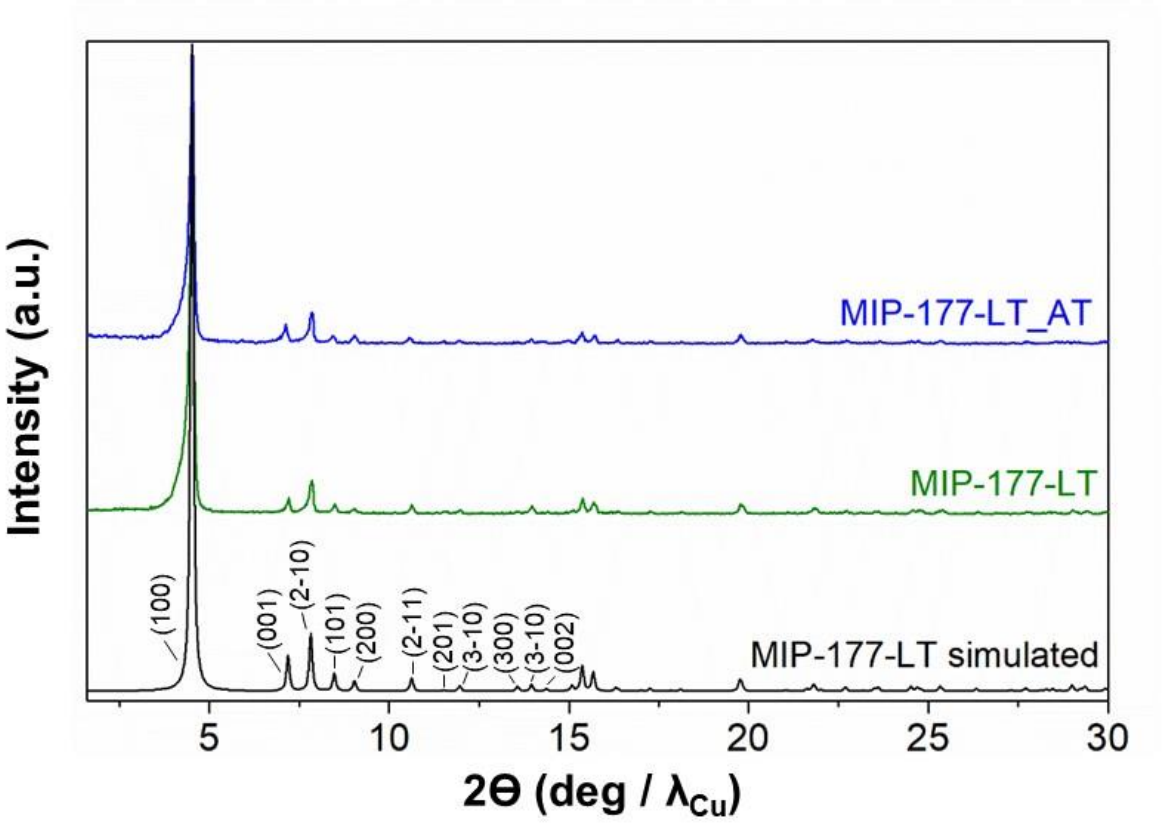


*Fig. 3. PXRD patterns of the pristine and the acid treated (AT) MIP-177-LT samples, in comparison with the simulated one for the crystal structure of MIP-177-LT in which the Miller indices are indicated for the first 10 reflections.*

*Photocatalytic stability.*

Prior to evaluation of the photocatalytic $H_2$ release from FA, blank controls irradiating MIP-177-LT and MIP-177-LT-AT photocatalysts were performed. These initial screening experiments serve to determine the photo stability of MIP-177-LT and MIP-177-LT-AT. Irradiations were carried out for 24 h periods as dry powders upon exposure to light of different wavelength regions. The results are summarized in Table S1. Previous reports in the literature have shown that carboxylate MOFs can undergo partial

photodecarboxylation under UV light in a significant extent of up to 33 % of the total carboxylate groups of the material during prolonged (months) irradiation times under UV-Vis light.[52]

In the present case, it was found that irradiation through Pyrex with the full spectral output of a 300 W Xe lamp for 24 h of 10 mg of MIP-177-LT gives rise to the evolution of 8 μmols $CO_2$ accompanied with two-orders of magnitude lesser amounts of $H_2$. This $CO_2$ evolution corresponds to about 8.8 % of the carboxylate groups present in the material according to its theoretical $Ti_{12}O_{15}(mdip)_3(formate)_6$ formula. In comparison, $CO_2$ evolution for the same period of time decreased by factors of 3.5 and 5.7 times less when the sample was irradiated with 360 and 400 nm cut-off filters, respectively. This corresponds to the photochemical decomposition in 24 h of 2.5 and 1.5 % of the carboxylate groups present in the material according to the theoretical formula, meaning that short wavelengths from 300 to 360 nm are responsible for most (71 %) of the MIP-177-LT self-decomposition and that irradiation with wavelengths longer than 400 nm diminishes MIP-177-LT damage in a 91 %.

Similar photostability studies were also performed on MIP-177-LT-AT. The same general trend, but with an even lesser $CO_2$ evolution (maximum of 2.00 μmol at 24 h) was observed. Incidentally, for MIP-177-LT-AT generation of $CH_4$ in higher proportion than the $H_2$ amounts was detected.

These preliminary studies indicate that deep UV radiation of wavelengths shorter than 360 nm is responsible for most of the $CO_2$ evolution and that part of these gases derive

from species present inside the channels that can be removed by acid treatment, since MIP-177-LT-AT has 70 % lesser $CO_2$ and $CH_4$ evolution. This less-damaging spectral range correspond to the solar spectrum at the earth surface.

To put into context these $CO_2$ evolution values with those that will be reported below in FA decomposition, they are three orders of magnitude lower and in the case of $H_2$ even lower. Therefore, the conclusion of these preliminary control studies is that self-decomposition is not relevant compared to the photocatalytic FA decomposition activity data presented herein below.

*$H_2$ release from photocatalytic FA decomposition.*

Photocatalytic $H_2$ release from FA experiments were carried out at room temperature under continuous magnetic stirring of 10 mg of either MIP-177-LT or MIP-177-LT-AT in 15 mL of $10^{-3}$ M FA solution in water in a closed 51 mL Pyrex reactor upon illumination of a 300 W Xe lamp (see Fig. S2). Gas evolution was periodically analyzed for 2 h irradiation runs by injecting the gases of the head space in a micro–GC. According to the dehydrogenation and dehydration reactions (eqs. 1 and 2), photocatalytic decomposition of FA can afford stoichiometric $H_2$ and $CO_2$ or stoichiometric $H_2O$ and CO, respectively. In agreement with the preliminary photo stability study, control experiments in the absence of FA under otherwise identical conditions or irradiation of FA in the absence of any MIP-177 photocatalysts show a negligible amount of $H_2$ compared to the large values observed for the FA solutions.

Noteworthy, the decomposition products observed in all the experiments with the presence of MIP-177 photocatalysts were predominantly $H_2$ and $CO_2$, accompanied with much lesser amounts of $CH_4$. Importantly, the amount of CO was below the detection limit of our GC analysis, corresponding to CO concentrations lower than 0.1 % in the gas composition, much smaller than the values about 10 % reported for $TiO_2$.[21, 39] 7.0 μmol $H_2$, corresponding to over 46 % of the theoretical stoichiometric amount for complete FA dehydrogenation (15 μmol) were quantified at 2 h of reaction time using fresh MIP-177-LT. Notably, while $H_2$ evolution increased quite linearly with the irradiation time, the $CO_2$ concentration profile slightly deviated from the $H_2$ one at shorter irradiation times, but finally both reached a quasi-stoichiometric amount at 2h reaction time. Fig. 4 A shows the time-evolution product formation measured for the fresh MIP-177-LT sample. Note that the continuous lines do not correspond to the fitting of the experimental points with the use of a kinetic model. In accordance with the expected influence of acid washings removing impurities, the photocatalytic activity of the acid treated MIP-177-LT-AT was even better and exhibit almost complete FA decomposition in 2 h with quasi-stoichiometric amounts of $H_2$ (13.0 $\mu molg^{-1}$) and $CO_2$ at 2 h irradiation time (Fig. 4 B and 4 C). Also, some methane formation was observed for MIP-177-LT, while in comparison the presence of methane in the case of MIP-177-LT-AT as photocatalyst was barely detectable.

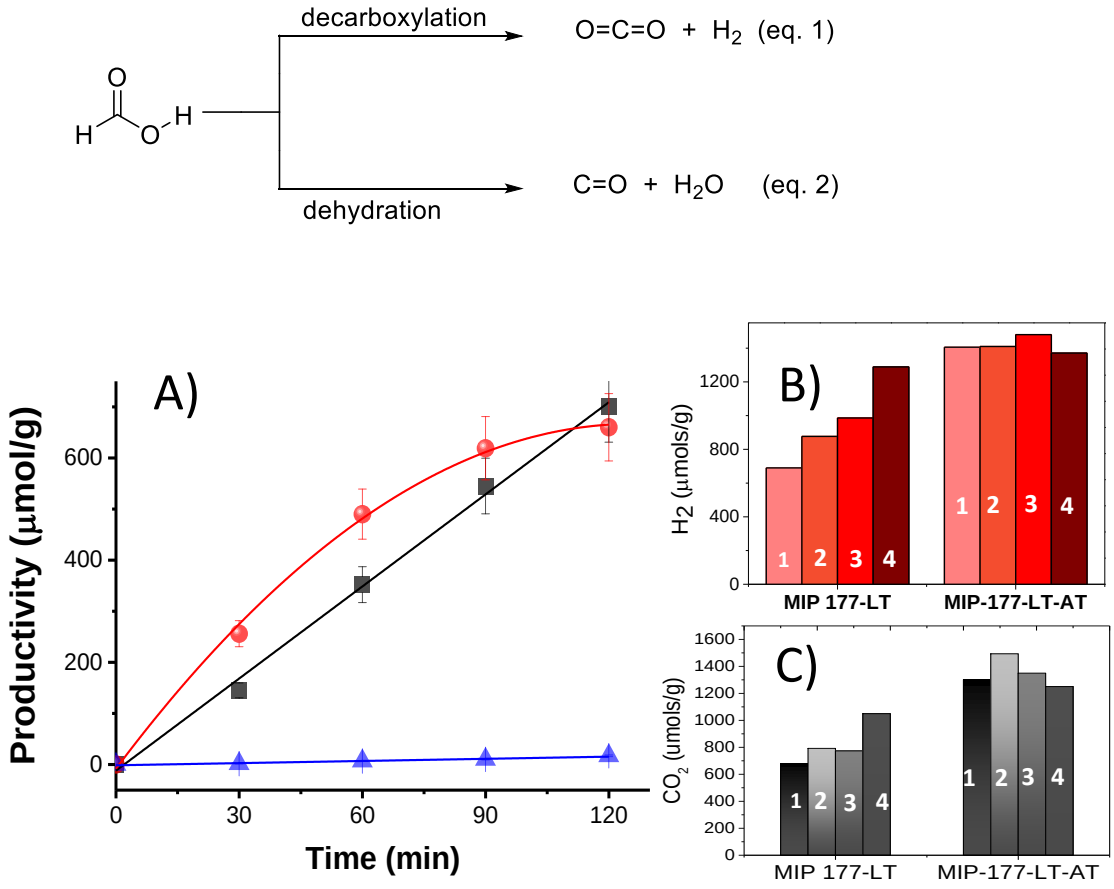


*Fig. 4. A) Time dependent profile of $H_2$ (black), $CO_2$ (red) and $CH_4$ (blue) upon UV-Vis irradiation of a $10^{-3}$ M FA aqueous solution in the presence of MIP-177-LT as photocatalyst. The continuous lines do not correspond to a fitting using a kinetic model. B) $H_2$ or $CO_2$ (C) production at 2 h irradiation time in the presence of MIP-177-LT or MIP-177-LT-AT upon the reuse number as indicated in the drawing. Reaction conditions: photocatalyst 10 mg, solution volume 20 mL, FA concentration $10^{-3}$ M, 300 W Xe lamp through Pyrex.*

Powder XRD and XPS data of the MIP-177-LT samples after the photocatalytic FA decomposition did not reveal any change (Fig. S3), confirming the excellent stability of the materials under the reaction conditions, in good accordance with the reported stability of MIP-177-LT under strongly acidic conditions. In addition, surface area measurements for the MIP-177-LT sample used as photocatalyst for $H_2$ release and exhaustive washing with water indicated a BET area of ### $m^2xg^{-1}$ that is somewhat lower than the value obtained

for the fresh material, but in line with that of MIP-177-LT-AT confirming porosity stability. Similarly, SEM images of the used MIP-177-LT sample (Fig. S3) show some abrasion of the particles that otherwise maintain the crystalline morphology of the fresh MIP-177-LT material.

In agreement with the catalyst stability in FA, reusability tests provided an important observation in the case of MIP-177-LT, i.e., $H_2$ and $CO_2$ evolution become faster and the final $H_2$ amount evolved at 2 h reaction time continuously grows upon reuse as presented in Fig. 4 B. Thus, the final $H_2$ amount increased from 700 $\mu mol \times g^{-1}$ to 877, 896 and 1289 $\mu mol \times g^{-1}$ for the first, second, third and fourth use, respectively. The $H_2$ amount released in the fourth use is about 86 % of the maximum theoretical $H_2$ amount according to the $10^{-3}$ M FA concentration. The apparent turnover frequency (TOF) obtained by dividing the evolved $H_2$ mols by the mols of Ti atoms present in the photocatalyst also grows from $2.5 \times 10^{-2}$ to 12.7 $10^{-2}$ $h^{-1}$ (see supporting information for details of apparent TOF calculation). As commented earlier and seen in Figure 4A, the use of fresh MIP-177-LT samples lead to a production of a higher $CO_2$ concentration than the corresponding stoichiometric $H_2$ amount at short reaction time. In comparison, as the same MIP-177-LT sample is increasingly reused, $CO_2$ evolution followed the same time-dependent profile as that $H_2$ and the amounts of evolved $CO_2$ and $H_2$ in the fourth use were even significantly higher than for the fresh MIP-177-LT sample. Therefore, the enhanced photocatalytic $CO_2$ evolution observed for the as-synthesized MIP-177-LT sample at initial reaction times is specific of this material and it tends to become corrected to the expected 1:1 $CO_2/H_2$ ratio upon extended irradiation. Furthermore, it is worth noting that acid-treated MIP-177-LT-TA sample exhibits a 1:1

$CO_2/H_2$ evolution since the start of the irradiation, meaning again that non-stoichiometric $CO_2/H_2$ evolution is exclusive of the fresh MIP-177-LT sample. Assuming that the charge separation state efficiency and other parameters related to the photocatalytic mechanisms dependent on the intrinsic electronic MIP-177-LT properties are constant upon reuse, TOF data indicate that about 5.1 more sites are becoming active upon MIP-177-LT reuse. This can be interpreted considering that only a fraction of the adjacent Ti atoms accessible from the pore space was initially available for the photocatalytic reaction in the fresh photocatalyst, and this percentage increases upon continuous irradiation, probably due to the decomposition of the structural formate groups bridging two equatorial Ti atoms of the same $Ti_{12}$ cluster. The TOF enhancement by a factor of about 5 upon reuse would indicate that for the extensively used MIP-177-LT electrons and holes located at any of the six positions of equatorial bridging formates accessible from the micropores have become photocatalytically active upon extended use, increasing in this way the efficiency of charge separation in the generation of $CO_2$ and $H_2$.

Notably, when considering the acid treated MIP-177-LT-AT that contains much less formates onto the $Ti_{12}O_{15}$ oxoclusters due to the acid treatment, the photocatalytic activity from the first to the fourth use becomes rather constant, although some increase in the TOF value from 0.35 $h^{-1}$ for the fresh sample to a TOF of 0.46 $h^{-1}$ for the fourth times used material was also observed. Most likely 0.46 $h^{-1}$ is about the maximum TOF value that can be achieved with the light power used in the present photocatalytic decomposition study. TOF values indicate that the performance of MIP-177-LT-AT is about four-fold higher than that of fresh MIP-177-LT, illustrating again the benefits of the acid treatment to achieve the

optimal photocatalytic activity. Interestingly, according to the stoichiometry of eq. 1 one can easily verify that a complete decomposition of all the FA present in the aqueous solution was achieved at 2 h irradiation for the MIP-177-LT-TA photocatalyst.

In addition, PXRD analysis after the five times used MIP-177-LT-AT sample did not reveal apparent change in the diffraction pattern compared to the fresh material (Fig. S4) again in accordance with the stability of MIP-177-LT in acid media.

*Benchmarking.*

To put the photocatalytic activity of MIP-177-LT and MIP-177-LT-TA into context, similar experiments on the photocatalytic $H_2$ release by FA decomposition were performed using the same mass of other benchmark MOFs photocatalysts, namely, MIL-125(Ti) and UiO-66(Zr). As commented earlier, to our knowledge, there are no precedents in the literature on the use of MOFs as the active photocatalyst for the photocatalytic FA decomposition, at the exception of a recent study from El Roz et al. based on UiO-66(Zr)-$(COOH)_2$. As summarized in Table 1, $H_2$ evolution was also observed for these MOFs with a final $H_2$ production at 2 h of 260 and 360 $\mu mol \times g_{photocatalyst}^{-1}$ for MIL-125(Ti) and UiO-66(Zr), respectively. This represents one half or less the photocatalytic activity of fresh MIP-177-LT and about seven times lower than that of highest performing MIP-177-LT-TA. Note that out of a few disordered defects, MIL-125(Ti) does not contain any structural site with formate imprinting. UiO-66(Zr) exhibits ordered or disordered sites, depending on the synthesis conditions, that are likely to be accessible to formate anchoring, but it is based on a different

coordination mode of the metal ($Zr^{4+}$ is 8 coordinated against 6-fold for $Ti^{4+}$ ions). Considering the unique structure of MIP-177-LT, we attribute this strong catalytic enhancement to the effect of the formate imprinting in the structure due to the specific arrangement of Ti atoms in the cluster. In comparison, the photocatalytic activity of MIL-125(Ti) and UiO-66(Zr) must correspond to the general electron/hole activity of photogenerated charge separate state to decompose FA.[53]

To further support that formate imprinting of $Ti_{12}O_{15}$ metal nodes in MIP-177-LT is responsible for this excellent performance in $H_2$ release from FA, photocurrent measurements using the same mass of the three MOFs were conducted. The results are presented in Fig. S5. As it can be seen, under the same conditions the photocurrent density of UiO-66 and MIL-125(Ti) was six and three times higher than that of MIP-177-LT respectively, meaning that the photogenerated charge carriers that can be extracted from these MOFs are higher than in MIP-177-LT. In spite of this lower charge extraction in MIP-177-LT, its photocatalytic activity for FA decomposition is much higher, indicating that the $Ti_{12}O_{15}$ oxo cluster organization is optimum to favor FA decomposition in spite of the lesser number of holes.

Table 1. Relative photocatalytic activity of reference photocatalysts compared to MIP-177-LT. *Reaction conditions: FA concentration $10^{-3}$ M, photocatalyst 10 mg, solution volume 15 mL, 300 W Xe lamp through Pyrex, reaction time 2 h.*

| Photocatalyts | $H_2$ production ($\mu mols \times g_{photocatalyst}^{-1}$) | TOF ($h^{-1}$) |
|---|---|---|
| MIL-125(Ti) | 266 | 0.021 |

| | | |
|---|---|---|
| UiO-66(Zr) | 360 | 0.031 |
| P-25 $TiO_2$ | 340 | 0.009 |
| MIP-177-LT-AT (fresh) | 1300 | 0.35 |

To consider a broader context, commercial P25 $TiO_2$ was finally evaluated as photocatalyst under the same conditions. Note that most of the studies with $TiO_2$ as photocatalyst use noble metal co-catalysts and herein the purpose was to evaluate the activity of plain $TiO_2$ that could be compared with the $Ti_{12}O_{15}$ clusters of MIP-177-LT. The results presented in Table 1 show that P25 exhibits a $H_2$ production at 2 h irradiation time similar to that measured for UiO-66(Zr), however it is much lower than those of the formate *imprinted* MIP-177-LT that upon reuse can be almost an order of magnitude more active than P25 $TiO_2$. Furthermore, apparent activation energy values ($E_a$) for the photocatalytic FA decomposition in the range of temperatures from 25 to 40 $^oC$ was determined for both MIP-177-LT and $TiO_2$ as photocatalysts. The results are presented in Fig. S6 in supplementary material. The corresponding $E_a$ values for MIP-177-LT and $TiO_2$ are 57.5 $kJmol^{-1}$ and 107.0 $kJmol^{-1}$, respectively. This trend clearly states that the FA decomposition is much more favorable in MIP-177-LT vs $TiO_2$.

*Influence of FA concentration.*

To take benefit from the exceptional chemical stability of MIP-177-LT in strong acid media, additional photocatalytic measurements were carried out with FA concentrations of

$10^{-2}$ and 1 M using MIP-177-LT as reference photocatalyst. The results summarized in Table S2 show that the $H_2$ evolution rate does not increase upon increasing FA concentration from $10^{-3}$ to $10^{-2}$ M. The highest concentration of 1 M, makes $H_2$ evolution even slower than when the concentration is $10^{-2}$ M. PXRD of the MIP-177-LT samples after their use as photocatalysts showed no appreciable changes in the PXRD patterns. Chemical analysis of the FA solution revealed an increase in the Ti content as a function of FA concentration that is <0.001, 0.012 and 4.86 % of the total Ti content present in the fresh MIP-177-LT used as photocatalyst for $10^{-3}$, $10^{-2}$ and 1 M FA solutions, respectively.

To understand the negative effect of excessive FA concentration, analogous studies on the influence of the concentration were carried out for aqueous solutions of sodium formate ($NaHCO_2$). The pH value of $NaHCO_2$ at $10^{-2}$ and 1 M was about neutral in the both cases. An increase in the temporal $H_2$ evolution plot upon increasing $NaHCO_2$ concentration in the $10^{-2}$ to 1 M was observed (Table 2). Accordingly, it is proposed that the MIP-177-LT structure is suitable to adsorb and recognize formate species, rather than FA. Adsorption of $HCO_2^-$ on the *imprinting* active sites results in an enhanced photocatalytic $H_2$ evolution.

Table 2. Photocatalytic $H_2$ release from sodium formate ($NaHCO_2$) as a function of the concentration. *Reaction conditions: FA concentration $10^{-3}$ M, photocatalyst 10 mg, solution volume 15 mL, 300 W Xe lamp through Pyrex, room temperature, reaction time 2 h.*

| | $H_2$ release ($\mu mol \times g_{photocatalyst}^{-1}$) | |
|---|---|---|
| Time | $NaHCO_2$ concentration $10^{-2}$ M | $NaHCO_2$ concentration 1 M |
| 30 | 120 | 280 |
| 60 | 324 | 645 |
| 90 | 430 | 916 |
| 120 | 870 | 1250 |

Now, when using aqueous FA solution and according to the equilibrium constant, formate should also be present when the concentration of FA in aqueous solution is $10^{-2}$ M and it is able to compete for the MIP-177 sites at this concentration. In contrast, the formate concentration becomes negligible compared to that of FA as the concentration of FA increases to 1 M. In addition, FA undergoes a strong association with the formation of FA dimers (eq. 3) at high concentration as observed in $^1H$ NMR spectroscopy.[54] These two

facts, the decrease in $HCO_2^-$ concentration relative to FA concentration and FA dimer association, are proposed to be responsible for the unexpectedly lower observed photocatalytic activity of MIP-177-LT as the FA concentration increases. Therefore, in agreement with the structure of MIP-177-LT these measurements clearly reveal that it is formate the real species that is undergoing decomposition by the imprinted adjacent bi Ti sites. The bidentate bridging of formate according to Fig. 1 justifies also the absence of CO formation that occur for monodentate FA bridging.[6]

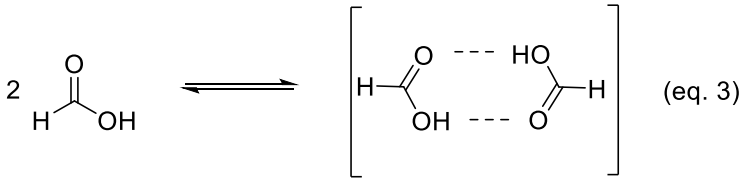


(eq. 3)

*Reaction mechanism.*

It is proposed that light absorption generates a transient state of charge separation resulting in electrons located at $Ti^{IV}$ and holes in oxygen atoms of the clusters and/or the mdip carboxylates. These holes at $Ti^{III}$ get one electron from formate promoting decarboxylation of attached $HCO_2\cdot$ radical intermediate, then evolving towards the formation of $CO_2$ as well as a surface H atom that will associate with an H atom generated by the reduction of $H^+$ by photogenerated electrons to form a $H_2$ molecule. Scheme 1 summarizes the possible mechanism along with the energy of the lowest unoccupied and highest occupied crystal orbitals (LUCO and HOCO) of MIP-177-LT vs the $H^+/H_2$ and $HCO_2H/CO_2$ redox potentials. The main peculiarity of MIP-177-LT compared to the other

two MOFs included in Table 1 is the presence of formate-imprinted sites in the structure that should favor adsorption of formates at the active site where holes are formed, thus increasing the efficiency of the process.

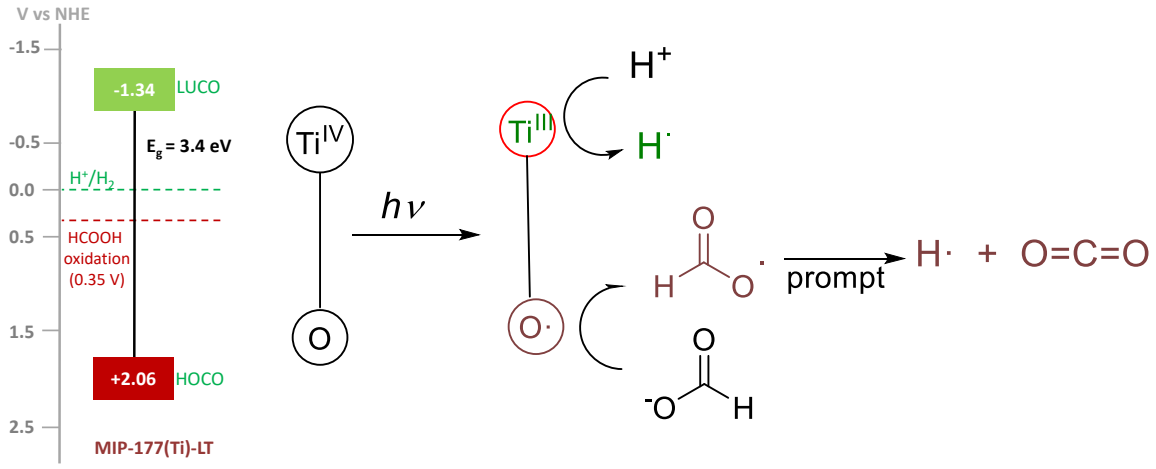


*Scheme 1. Proposed reaction mechanism. Upon light absorption, an electron migrates by ligand-to-metal photoinduced charge transfer to the $Ti^{IV}$. Photogenerated electrons on $Ti^{III}$ produce H atoms and photogenerated holes produce formate radicals that decompose to $CO_2$ and H atoms.*

To support this possible mechanism, photocatalytic formate decomposition was performed in the presence of quenchers. Table S3 provides a summary of the quenching study. In this way, performing the photocatalytic formic acid decomposition in the presence of $10^{-3}$ M of cerium ammonium nitrate results in a significant diminution of the amount of evolved $H_2$ to about one third of the volume in the absence of $Ce(NH_4)_2(NO_3)_6$, while $CO_2$ evolution was enhanced somewhat from 701 to 794 $\mu molg_{photocatalyst}$ at 2 h reaction time. This observation is compatible with the mechanistic proposal, holes being consumed by formates evolving $CO_2$, while photogenerated electrons convert $Ce^{IV}$ into $Ce^{III}$, thwarting in part $H_2$ evolution that becomes unbalanced.

In contrast, all the attempts to stop or diminish $CO_2$ evolution in MIP-177-LT as reference photocatalyst by using hole quenchers such as hydrogen sulfite or hydrogen sulfide were unsuccessful (Table S4), probably reflecting the preferential selective formate adsorption on the Ti atoms respect to the quenchers.

*Molecular insights into the reaction mechanism*

Density functional theory (DFT) calculations implementing D3 dispersion correction (see supporting information) were further performed to shed light on the catalytic reaction mechanism and to understand the electronic and structural origins of the outstanding performance exhibited by MIP-177(Ti)-LT. Herein, a representative $Ti_{12}O_{15}$ cluster model was cleaved from the periodic MOF structure integrating an unsaturated $Ti^{IV}/Ti^{III}$ pair to account for the light-induced switching of one active site from $Ti^{IV}$ to $Ti^{III}$ as revealed experimentally and in line with previously reported Ti-MOFs.[55, 56] The first step of the reaction, i.e. chemisorption HCOOH throughout this Ti active site, is associated with an adsorption energy of -0.79 eV and Ti-O(HCOOH) distances of 2.65 Å ($Ti^{III}$) and 2.61 Å ($Ti^{IV}$) (Table S5) that suggests a favorable formation of this initial state, although without leading to a highly stable state that would be detrimental to proceed the following steps of the mechanism. The calculated Gibbs-free energy profile for the dehydrogenation of *HCOOH through the *HCOO (formate) pathway was further explored (Fig. 5a) and was found to be more thermodynamically favorable as compared to the dehydration process examined in Fig. S7. The adsorbed *HCOOH molecule undergoes O–H bond cleavage to form *HCOO* and *H first. At this step, the released H is coordinated to the $\mu_O$ site, while O of *HCOO*

still bonds to the Ti site. Then, *HCOO undergoes a reorientation and the C-H bond breaks to form $CO_2$.

For comparison, the $TiO_2$ (110) as benchmark photocatalyst was also computationally explored. We first calculated that the adsorption energy of HCOOH (-1.49 eV) on $TiO_2$ (110) is much higher than that calculated for MIP-177(Ti)-LT (-0.79 eV) in line with substantially shorter Ti-O(HCOOH) distances (2.10 Å and 2.18 Å vs 2.65 Å and 2.61 Å for MIP-177(Ti)-LT) (details shown in Table S5). The adsorption of *HCOO is also more energetics on $TiO_2$ (110) surface than that of MIP-177(Ti)-LT (energy difference: 0.76 eV), which makes the cleavage of the C–H bond from *HCOO much less thermodynamically preferable on $TiO_2$ ($\Delta G$=1.34 eV) compared to MIP-177(Ti)-LT ($\Delta G$=0.35 eV) as revealed in Fig. 5a. This predicted trend is in line with the much lower activation energy value measured for the photocatalytic FA decomposition in MIP-177-LT (57.5 $kJmol^{-1}$) vs $TiO_2$ (107.0 $kJmol^{-1}$). The local environment of $Ti_{12}O_{15}$ inorganic node of MIP-177(Ti)-LT combined with its structural adaptability towards guest adsorption (see the guest-induced structure relaxation in Fig. S8 and Table S5) is a key to offer an optimum energetics for the coordination of *HCOOH and *HCOO to promote an effective catalytic activity according to the Sabatier principle.[57]

According to the Gibbs-free energy profile, the C-H cleavage of *HCOO is the key step for $H_2$ release reaction. We analyzed the crystal orbital Hamilton populations (COHP) for *HCOO adsorption configuration and we found that the interaction between *HCOO and MIP-177(Ti)-LT comes from the anti-bonding between O of *HCOO and Ti of MIP-177(Ti)-LT (Fig. 5b). In addition, for MIP-177(Ti)-LT, the charge density difference analysis

clearly showed that there is an accumulation of electrons on the Ti atom and depletion on the O atom (Fig. 5c). This electronic transfer is at the origin of the relative strong interaction between the Ti and O atoms, beneficial for the following transformation of electrons to the C atom, promoting the cleavage of C-H. The density of states (DOS) analysis (Fig. 5d) evidenced that the O-*p* states contribute to the lowest unoccupied molecular orbital (LUMO) which accept electrons, while Ti-*d* states contribute to the highest occupied molecular orbital (HOMO) which provide electrons. The same conclusion can be drawn from the analysis of the *HCOOH adsorption configuration (Fig. S9). This whole analysis supports that the light-induced $Ti^{III}$ plays a critical role in the whole photocatalytic FA decomposition of MIP-177(Ti)-LT.

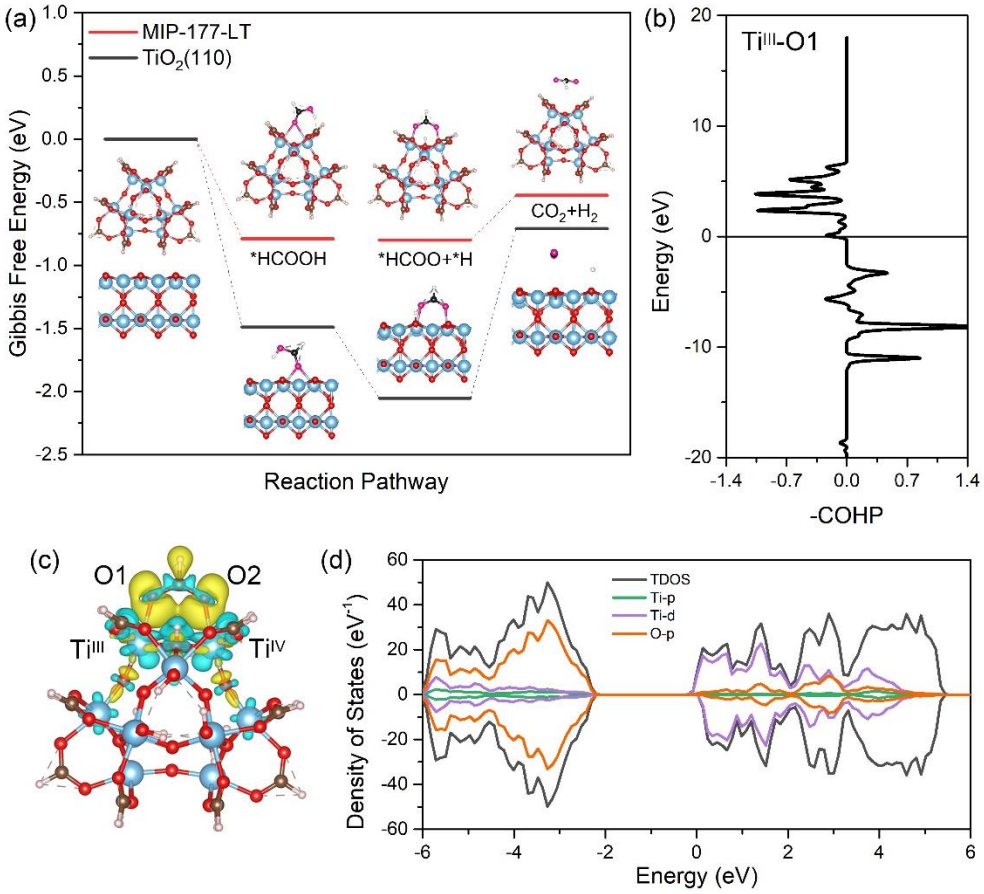


*Fig. 5. (a) Gibbs free energy profile for the conversion HCOOH into $H_2$ and $CO_2$ simulated for MIP-177(Ti)-LT and $TiO_2$ (110). The total free energy of MIP-177(Ti)-LT and $TiO_2$ models with gas-phase HCOOH molecule was set as the zero point in the energy profile. The color scheme for FA: O, pink; H, white; C, black; The color scheme for catalysts: Ti, blue; O, red; H: light pink. (b) COHP analysis of *HCOO on MIP-177-LT for $Ti^{III}$ adsorption site. Positive and negative values of –COHP correspond to bonding and antibonding interactions. (c) Charge density difference of *HCOO on MIP-177(Ti)-LT cluster model. Yellow and blue lobes refer to electron accumulation and depletion regions. (d) Total and projected Density of States (DOS) of *HCOO on MIP-177(Ti)-LT cluster model.*

*Photo response of MIP-177-LT*

Further studies were aimed at determining the chromophores responsible for the photodecarboxylation by studying the influence of the irradiation wavelength in $H_2$ release from FA using MIP-177-LT as photocatalyst. The results are presented in Fig. 6. It can be seen that irradiation in the deep UV at 238 nm exhibits a high apparent quantum yield of 22 %. This remarkable quantum yield decreases as the irradiation wavelength becomes longer. At 300 nm, the apparent quantum yield is 0.5 %. This dependency of the photocatalytic activity with the wavelength indicates that direct excitation of Ti←O ligand-to-metal charge transfer band of $Ti_{12}O_{15}$ clusters that should have an absorption band at 240 nm is the most efficient photophysical process to promote FA decarboxylation and $H_2$ release. [58, 59] Excitation at the localized organic mdip linker with absorption extending to 274 and 300 nm can also promote $H_2$ evolution through a $Ti_{12}O_{15}$←mdip ligand to metal charge transfer,[56] but with much less efficiency. This lesser efficiency indicates the incomplete quenching of localized mdip excitons by the $Ti_{12}O_{15}$ cluster, probably because other deactivation pathways are available to the ligand excited state including radiationless decay through conformational phenyl ring rotation or emissive photoluminescence.

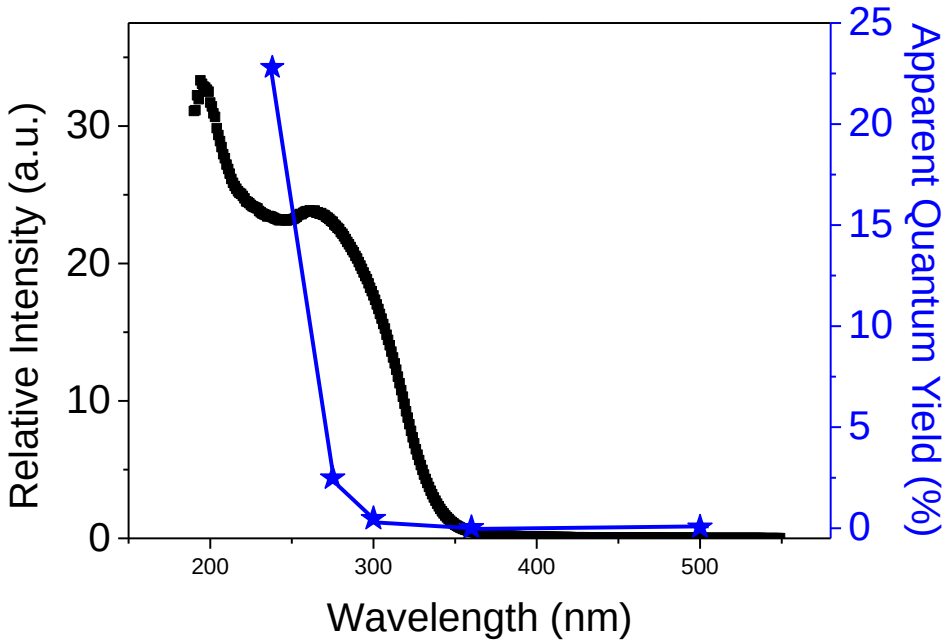


*Fig. 6. Photoresponse MIP-177-LT for FA decarboxylation at different wavelengths (left axis) compared with the diffuse reflectance UV-Vis absorption spectrum for MIP-177-LT.*

Photoresponse in the visible, although existing in MIP-177-LT, probably due to the action of structural defects or impurities, is orders of magnitude lower that in the UV. In fact, one of the improvements to increase photocatalytic activity of MIP-177-LT could be extending its photoresponse towards longer wavelengths by appropriate design of mixed metal or mixed ligand MIP-177 following reported strategies.

*Scope.*

Photocatalytic decarboxylation is a general reaction that has gained renewed interest as a way to obtain hydrocarbon fuels from biomass-derived aliphatic carboxylic

acids.[60, 61] As FA, other carboxylic acids can undergo photocatalytic decarboxylation to form the corresponding alkyl radicals that can abstract one hydrogen from the solvent, dimerize or undergo trapping after consecutive reactions.[60, 62, 63] It was of interest to determine, whether or not the formate-imprinted photocatalytic site of MIP-177-LT can also promote photodecarboxylation of other carboxylic acids with similar high activity. Therefore, besides FA decomposition, the photocatalytic activity of MIP-177-LT was also assessed in the photocatalytic decarboxylation of acetic, propionic and methacrylic acids.

As expected, all the tested aliphatic carboxylic acids undergo photodecarboxylation promoted by MIP-177-LT. The main product was $CO_2$, accompanied by much lesser amounts of $H_2$ and light alkanes. The results are presented in Table 3. As it can be seen there, acetic acid at $10^{-3}$ M concentration undergoes a complete photocatalytic decarboxylation after 16 h irradiation time. The initial evolution of $H_2$ during the irradiation indicates that formate groups present in MIP-177-LT are undergoing photodecarboxylation in the first stages, before observing acetic acid decarboxylation. Interestingly, a second use of the MIP-177-LT shows a considerable deactivation degree of about 90 % that further decreases to a residual 5 % of the initial activity in the third use. This behavior contrasts to the previously commented growth in MIP-177-LT catalytic activity using FA and indicates the poisoning of the active sites by some blocking by-products. The fact that methane is not evolved in the expected stoichiometric amounts respect to $CO_2$ suggest that some by product such as methoxy groups could be blocking the sites.

Propanoic acid also undergoes photodecarboxylation in a considerable extent after 2 h of 300 W Xe lamp irradiation (Table 3) and undergoes deactivation in the second use to

a value corresponding to only about 20 % of the activity of the fresh MIP-177-LT. Although the origin of deactivation deserves a deeper study, PXRD of the deactivated MIP-177-LT after its use as photocatalyst shows that the crystallinity of the samples has been preserved, indicating that MIP-177-LT decomposition is not the reason of the loss of photocatalytic activity.

Similar trends were also observed for the photocatalytic decomposition of methacrylic acid promoted by MIP-177-LT, i.e., evolution of CO2 without being accompanied of similar proportions of other organic hydrocarbons and considerable deactivation upon reuse.

Although further studies are necessary to understand the photocatalytic data and performance of MIL-177-LT for acetic, propionic and methacrylic acid, the behavior with these carboxylic acids clearly contrasts with that of FA, thus reinforcing the importance of formate imprinting on the $Ti_{12}O_{15}$ nodes on the photocatalytic $H_2$ release activity and stability.

Table 3. Products and $H_2$ evolution upon irradiation of carboxylic acids using MIP-177-LT as photocatalysts. Reaction conditions: 15 mL aqueous solution of 10-3 M carboxylic acid, MIP-177-LT 10 mg, 300 W Xe lamp, reactor volume 51 mL, time 2 h.

| Carboxylic acid | $H_2$ ($\mu mol \times g_{photocatalyst}^{-1}$) | $CO_2$ ($\mu mol \times g_{photocatalyst}^{-1}$) | Other |
|---|---|---|---|

| | | | |
|---|---|---|---|
| Acetic acid<br>16 h | 1350 | 1405 | $CH_4$ |
| Propionic acid<br>2 h | 1487 | 922 | $CH_4$, $CH_3CH_3$ |
| Methacrylic acid | 1410 | 1490 | $CH_4$, $CH_3$-CH=$CH_2$ |

**Conclusions.**

Ti-MOF MIP-177-LT was demonstrated to combine several properties that makes this material highly active for the photocatalytic $H_2$ release from FA, specially the presence of accessible formate-imprinted active sites in equatorial Ti atoms and its structural robustness in strong acid media. These unique features led to a FA decomposition activity over one order of magnitude superior to the ones of the benchmark MOF photocatalysts MIL-125(Ti) and UiO-66(Zr) or over 30 times that of $TiO_2$ P25, reaching an apparent quantum yield as high as 22 % in the UV. Noteworthy, the FA photocatalytic decomposition rate of the fresh MIP-177-LT increases upon irradiation and is disfavored at high FA concentrations, facts that are related to the preference of the material for formate respect to its acid form. Acid washing has a beneficial influence on the photocatalytic activity of MIP-177-LT-AT by removing impurities and releasing the active centers, reaching a maximum TOF value of 0.46 $h^{-1}$. Quenching studies and DFT calculations support that $H_2$ consumes photogenerated electrons, but $CO_2$ evolution could not be quenched by strong electron donors indicating the high selectivity of the active sites for formate coordination. Considering the advantage

of light over heat for instantaneous on-off control of $H_2$ release, the present results open the way for efficient MOF photocatalysts by design based on earth abundant and affordable elements.

**Acknowledgements.**

Financial support by the Spanish Ministerio de Ciencia e Innovación (PID2021-126071OB-C21 and Severo Ochoa) and Generalitat Valenciana (Prometeo 2017/083) is gratefully acknowledged. R. D. A. is thankful to CONACYT for the PhD grant 2018-000003-01EXTF-00075 (CVU: 697332).

**References.**

[1] Z. Abdin, A. Zafaranloo, A. Rafiee, W. Mérida, W. Lipiński, K. R. Khalilpour, *Renewable and sustainable energy reviews* **2020**, *120*, 109620.
[2] S. Sharma, S. K. Ghoshal, *Renewable and sustainable energy reviews* **2015**, *43*, 1151-8.
[3] T. He, Q. Pei, P. Chen, *Journal of energy chemistry* **2015**, *24*, 587-94.
[4] D. Teichmann, W. Arlt, P. Wasserscheid, R. Freymann, *Energy & Environmental Science* **2011**, *4*, 2767-73.
[5] M. Grasemann, G. Laurenczy, *Energy & Environmental Science* **2012**, *5*, 8171-81.
[6] K. Tedsree, T. Li, S. Jones, C. W. A. Chan, K. M. K. Yu, P. A. J. Bagot, E. A. Marquis, G. D. W. Smith, S. C. E. Tsang, *Nature Nanotechnology* **2011**, *6*, 302-7.
[7] S. Fukuzumi, T. Kobayashi, T. Suenobu, *ChemSusChem: Chemistry & Sustainability Energy & Materials* **2008**, *1*, 827-34.
[8] Y. Himeda, *Green Chemistry* **2009**, *11*, 2018-22.
[9] S.-M. Lu, Z. Wang, J. Wang, J. Li, C. Li, *Green Chemistry* **2018**, *20*, 1835-40.
[10] Z. L. Wang, J. M. Yan, Y. Ping, H. L. Wang, W. T. Zheng, Q. Jiang, *Angewandte Chemie* **2013**, *125*, 4502-5.
[11] Q. Zhang, Q. Mao, Y. Zhou, L. Zou, D. Zhu, Y. Huang, H. Gao, X. Luo, Y. Mao, Z. Liang, *ACS Sustainable Chemistry & Engineering* **2022**, *10*, 4599-609.
[12] D. Mellmann, E. Barsch, M. Bauer, K. Grabow, A. Boddien, A. Kammer, P. Sponholz, U. Bentrup, R. Jackstell, H. Junge, *Chemistry–A European Journal* **2014**, *20*, 13589-602.

[13] D. Mellmann, P. Sponholz, H. Junge, M. Beller, *Chemical Society Reviews* **2016**, *45*, 3954-88.
[14] A. Léval, A. Agapova, C. Steinlechner, E. Alberico, H. Junge, M. Beller, *Green Chemistry* **2020**, *22*, 913-20.
[15] N. Onishi, G. Laurenczy, M. Beller, Y. Himeda, *Coordination Chemistry Reviews* **2018**, *373*, 317-32.
[16] V. Singh, R. Singh, *Corrosion Science* **1995**, *37*, 1399-410.
[17] K. Grubel, H. Jeong, C. W. Yoon, T. Autrey, *Journal of Energy Chemistry* **2020**, *41*, 216-24.
[18] K. Sordakis, A. F. Dalebrook, G. Laurenczy, *ChemCatChem* **2015**, *7*, 2332-9.
[19] J. r. Eppinger, K.-W. Huang, *ACS Energy Letters* **2017**, *2*, 188-95.
[20] B. M. Besancon, V. Hasanov, R. Imbault-Lastapis, R. Benesch, M. Barrio, M. J. Mølnvik, *International Journal of Hydrogen Energy* **2009**, *34*, 2350-60.
[21] M. Navlani-García, D. Salinas-Torres, K. Mori, Y. Kuwahara, H. Yamashita, *Heterogeneous Photocatalysis* **2020**, 193-223.
[22] H. J. Yun, H. Lee, J. B. Joo, W. Kim, J. Yi, *The Journal of Physical Chemistry C* **2009**, *113*, 3050-5.
[23] Z. Zhang, S.-W. Cao, Y. Liao, C. Xue, *Applied Catalysis B: Environmental* **2015**, *162*, 204-9.
[24] Y. Ji, Y. Luo, *Journal of Power Sources* **2016**, *306*, 208-12.
[25] A. Gazsi, G. Schubert, P. Pusztai, F. Solymosi, *International journal of hydrogen energy* **2013**, *38*, 7756-66.
[26] C. Tao, W. Guopeng, F. Zhaochi, H. Gengshen, S. Weiguang, Y. Pinliang, L. Can, *Chinese Journal of Catalysis* **2008**, *29*, 105-7.
[27] K. L. Miller, C. W. Lee, J. L. Falconer, J. W. Medlin, *Journal of Catalysis* **2010**, *275*, 294-9.
[28] B. Wu, J. Lee, S. Mubeen, Y. S. Jun, G. D. Stucky, M. Moskovits, *Advanced Optical Materials* **2016**, *4*, 1041-6.
[29] I. Willner, Z. Goren, *Journal of the Chemical Society, Chemical Communications* **1986**, 172-3.
[30] S. Cao, Y. Chen, H. Wang, J. Chen, X. Shi, H. Li, P. Cheng, X. Liu, M. Liu, L. Piao, *Joule* **2018**, *2*, 549-57.
[31] R. Zhu, F. Tian, R. Yang, J. He, J. Zhong, B. Chen, *Renewable Energy* **2019**, *139*, 22-7.
[32] M. Hamandi, G. Berhault, C. Guillard, H. Kochkar, *Applied Catalysis B: Environmental* **2017**, *209*, 203-13.
[33] Q. Zhang, C.-F. Lin, Y. H. Jing, C.-T. Chang, *Journal of the Air & Waste Management Association* **2014**, *64*, 578-85.
[34] M. Hamandi, G. Berhault, C. Guillard, H. Kochkar, *Molecular Catalysis* **2017**, *432*, 125-30.
[35] C. Wan, L. Zhou, L. Sun, L. Xu, D.-g. Cheng, F. Chen, X. Zhan, Y. Yang, *Chemical Engineering Journal* **2020**, *396*, 125229.
[36] A. Dhakshinamoorthy, Z. Li, H. Garcia, *Chemical Society Reviews* **2018**, *47*, 8134-72.
[37] A. Dhakshinamoorthy, A. M. Asiri, H. Garcia, *Angewandte Chemie International Edition* **2016**, *55*, 5414-45.
[38] X. Deng, Z. Li, H. García, *Chemistry–A European Journal* **2017**, *23*, 11189-209.
[39] M. Zeng, Z. Chai, X. Deng, Q. Li, S. Feng, J. Wang, D. Xu, *Nano Research* **2016**, *9*, 2729-34.
[40] M. Wen, K. Mori, Y. Kuwahara, H. Yamashita, *ACS Energy Letters* **2017**, *2*, 1-7.
[41] M. Zhang, W. Lin, L. Ma, Y. Pi, T. Wang, *Chemical Communications* **2022**, *58*, 7140-3.
[42] D. Jiang, C. Huang, J. Zhu, P. Wang, Z. Liu, D. Fang, *Coordination Chemistry Reviews* **2021**, *444*, 214064.
[43] N. Stock, S. Biswas, *Chemical reviews* **2012**, *112*, 933-69.

[44] S. A. Younis, E. E. Kwon, M. Qasim, K.-H. Kim, T. Kim, D. Kukkar, X. Dou, I. Ali, *Progress in Energy and Combustion Science* **2020**, *81*, 100870.
[45] M. Ghorbanloo, V. Safarifard, A. Morsali, *New Journal of Chemistry* **2017**, *41*, 3957-65.
[46] J. Sun, J. Wan, Y. Wang, Z. Yan, Y. Ma, S. Ding, M. Tang, Y. Xie, *Journal of Hazardous Materials* **2022**, *429*, 128299.
[47] G. Wißmann, A. Schaate, S. Lilienthal, I. Bremer, A. M. Schneider, P. Behrens, *Microporous and Mesoporous Materials* **2012**, *152*, 64-70.
[48] H. Assi, G. Mouchaham, N. Steunou, T. Devic, C. Serre, *Chemical Society Reviews* **2017**, *46*, 3431-52.
[49] S. Wang, T. Kitao, N. Guillou, M. Wahiduzzaman, C. Martineau-Corcos, F. Nouar, A. Tissot, L. Binet, N. Ramsahye, S. Devautour-Vinot, S. Kitagawa, S. Seki, Y. Tsutsui, V. Briois, N. Steunou, G. Maurin, T. Uemura, C. Serre, *Nature communications* **2018**, *9*, 1660-.
[50] S. Nandi, S. Wang, M. Wahiduzzaman, V. Yadav, K. Taksande, G. Maurin, C. Serre, S. Devautour-Vinot, *ACS Applied Materials & Interfaces* **2021**, *13*, 20194-200.
[51] R. V. Pinto, S. Wang, S. R. Tavares, J. Pires, F. Antunes, A. Vimont, G. Clet, M. Daturi, G. Maurin, C. Serre, *Angewandte Chemie International Edition* **2020**, *59*, 5135-43.
[52] D. Mateo, A. Santiago‐Portillo, J. Albero, S. Navalón, M. Alvaro, H. García, *Angewandte Chemie* **2019**, *131*, 18007-12.
[53] M.-Y. Qi, M. Conte, M. Anpo, Z.-R. Tang, Y.-J. Xu, *Chemical Reviews* **2021**.
[54] W. Reutemann, H. Kieczka, *Ullmann's encyclopedia of industrial chemistry* **2011**, *1*.
[55] M. de Miguel, F. Ragon, T. Devic, C. Serre, P. Horcajada, H. García, *ChemPhysChem* **2012**, *13*, 3651-4.
[56] A. Santiago Portillo, H. G. Baldoví, M. T. Garcia Fernandez, S. Navalon, P. Atienzar, B. Ferrer, M. Alvaro, H. Garcia, Z. Li, *The Journal of Physical Chemistry C* **2017**, *121*, 7015-24.
[57]
[58] A. Dhakshinamoorthy, S. Navalon, A. Corma, H. Garcia, *Energy & Environmental Science* **2012**, *5*, 9217-33.
[59] C. Aprile, A. Corma, H. Garcia, *Physical Chemistry Chemical Physics* **2008**, *10*, 769-83.
[60] D. Budac, P. Wan, *Journal of Photochemistry and Photobiology A: Chemistry* **1992**, *67*, 135-66.
[61] X. Du, Y. Peng, J. Albero, D. Li, C. Hu, H. García, *ChemSusChem* **2022**, *15*, e202102107.
[62] J. Schwarz, B. König, *Green Chemistry* **2018**, *20*, 323-61.
[63] J. Shi, T. Yuan, M. Zheng, X. Wang, *ACS Catalysis* **2021**, *11*, 3040-7.